inorganics

MDPI

Article

Study of the Cathode Pt-Electrocatalysts Based on Reduced Graphene Oxide with Pt-SnO_2 Hetero-Clusters

Dmitry D. Spasov [1,2,*], Nataliya A. Ivanova [1], Ruslan M. Mensharapov [1], Matvey V. Sinyakov [1,3], Adelina A. Zasypkina [1], Elena V. Kukueva [1], Alexander L. Trigub [1], Elizaveta S. Kulikova [1] and Vladimir N. Fateev [1]

1 National Research Center "Kurchatov Institute", 1, Akademika Kurchatova Sq., 123182 Moscow, Russia; ivanovana.1989@outlook.com (N.A.I.); mensharapov_rm@nrcki.ru (R.M.M.); mmatveimatvei4@gmail.com (M.V.S.); zasypkina_aa@nrcki.ru (A.A.Z.); elena.kukueva@gmail.com (E.V.K.); alexander.trigub@gmail.com (A.L.T.); lizchkakul@mail.ru (E.S.K.); vladimirfateev2@yandex.ru (V.N.F.)

2 Department of Chemistry and Electrochemical Energy, National Research University "Moscow Power Engineering Institute", 14, Krasnokazarmennaya St., 111250 Moscow, Russia

3 Institute of Modern Energetics and Nanotechnology, D. Mendeleev University of Chemical Technology of Russia, 9, Miusskaya Square, 125047 Moscow, Russia

* Correspondence: spasovdd@outlook.com

Abstract: A complex study of the structure, morphology, and electrochemical properties of the $Pt^{20}/SnO_2{}^{10}$/RGO electrocatalyst is presented. The advantage of the chemical synthesis of reduced graphene oxide (c-RGO) compared to thermal methods (t-RGO) is due to the formation of graphene plates with amorphous carbon black agglomerates and the chemical composition of the surface. The nature of the interaction between platinum and tin dioxide particles and a conclusion about the formation of heterostructures Pt-SnO_2 with the surface interaction of lattices excluding the formation of hetero phases has been established. This achieves high dispersity during the formation of platinum particles without significant agglomeration and increases the electrochemical surface area (ESA) of platinum to 85 $m^2\ g^{-1}$ vs. carbon black. In addition, the surface interaction of particles and the formation of hetero-clusters Pt-SnO_2 can cause the improved activity and stability of the $Pt^{20}/SnO_2{}^{10}$/c-RGO electrocatalyst.

Keywords: PEM fuel cell; Pt-SnO_2 hetero-clusters; electrocatalysts; reduced graphene oxide; catalyst stability; catalyst activity

check for updates

Citation: Spasov, D.D.; Ivanova, N.A.; Mensharapov, R.M.; Sinyakov, M.V.; Zasypkina, A.A.; Kukueva, E.V.; Trigub, A.L.; Kulikova, E.S.; Fateev, V.N. Study of the Cathode Pt-Electrocatalysts Based on Reduced Graphene Oxide with Pt-SnO_2 Hetero-Clusters. *Inorganics* **2023**, *11*, 325. https://doi.org/10.3390/inorganics11080325

Academic Editors: Guido Kickelbick, Gary Hix, Richard Dronskowski, Christian Julien, Rainer Niewa, Alexander Novikov and Hans-Conrad zur Loye

Received: 13 June 2023
Revised: 17 July 2023
Accepted: 28 July 2023
Published: 31 July 2023

1. Introduction

Pt-based electrocatalysts are commonly used for proton-exchange membrane (PEM) fuel cells (FCs). Corrosion resistance is an important characteristic of suitable catalyst support, along with high electrical conductivity, high surface area, hydrophobicity, morphology, porosity, etc. This promising strategy aimed to mitigate carbon support limitations using carbon-based hybrid supports [1].

A complete rejection of Pt as an active component of PEMFC electrocatalysts seems premature, but a promising direction is the use of multicomponent complex systems, for example, platinum–tin dioxide (Pt-SnO_2) clusters based on carbon support [2–4]. Tin oxide–carbon composites demonstrate high chemical and electrochemical stability, along with a strong interaction with supported metal nanoparticles [5]. The high durability of the Pt-SnO_2-based catalysts is attributed to the strong metal–support interaction (SMSI) that inhibits the migration and agglomeration of the nanoparticles at the electrode surface. Previously, it was shown that the $Pt^{20}/SnO_2{}^{10}$/C electrocatalyst demonstrates increased stability during accelerated stress tests (AST) due to the high stability of SnO_2 particles (10 wt.%) and their interaction with Pt [6,7]. However, the use of SnO_2 lowers both the electrical conductivity of the electrocatalyst due to the semiconductor properties of SnO_2 and the electrochemical surface area (ESA) due to the high degree of particle agglomeration.

An increase in the electrical conductivity and specific surface area of the catalyst can be achieved using complex carbon supports, which have a high specific surface area and increased electrical conductivity compared to amorphous carbon black. In this case, reduced graphene oxide (RGO) is a promising material for electrochemical power engineering due to its large specific surface area, high stability, and electrical conductivity [1]. RGO consists of plates of partially oxidized graphene, the basal planes of which are decorated with epoxy and hydroxyl groups, in addition to carbonyl and carboxyl groups located at the edges. RGO, in the physicochemical sense, is not equal to graphene; in other words, it is not possible to completely reduce graphite oxide (GO) to graphene. Thus, the products obtained during its reduction contain significant amounts of oxygen [8]. RGO is obtained in several stages, from graphite to GO to reduced graphene oxide. There are several methods for synthesizing GO, such as the Brodie method, the Staudenmaier method, and the Hummers method and its variants (the modified and improved Hummers method) [9,10].

RGO can be obtained directly by removing oxygen functional groups from GO according to various strategies: thermal reduction, photoreduction, electrochemical reduction, microwave reduction, solvothermal reduction, and chemical reduction using a wide range of reducing agents (hydroiodic acid, ascorbic acid, hydrazine, $NaBH_4$ or hydrides of some metals) and multiphase recovery [11–18]. The resulting compounds can be used as supports for FC electrocatalysts. In [19–22], the electrochemical properties of the RGO catalyst were studied, showing a high ESA and stability in AST.

At present, complex multicomponent Pt (or Pd)/SnO_2/RGO catalysts are being studied in various fields as gas-sensitive materials in gas sensors [23–26] and electrocatalysts for direct methanol fuel cells (DMFC) [27,28].

In [29], a hierarchically structured Pt/SnO_2/RGO electrocatalyst was developed using layer-by-layer synthesis. A morphologically controlled synthesis was used to obtain regularly shaped SnO_2 crystallites, including specific faces such as (101), (110), (111), and (221). Next, Pt nanoparticles were uniformly deposited on different faces of SnO_2. The use of RGO made it possible to obtain an electrocatalyst with improved electronic conductivity and stability. The authors of [30] studied a series of Pt/SnO_2/RGO electrocatalysts with a low Pt content (0.77, 0.89, and 1.21 wt.%). The photo-excited in situ loading of Pt clusters onto RGO-immobilized SnO_2 was used in this work. The authors of [31] used the photo-assisted reduction method as an addition to traditional chemical reduction to obtain a well-hierarchical heterostructure of Pt@SnO_2/graphene. The photo-assisted reduction method is an important method for regulating the interfacial interaction of active substances in hybrid electrocatalysts. As a result, the electrocatalyst exhibited significantly improved catalytic activity and increased cyclic stability. In studies [32], electrochemically exfoliated graphene (EEG) was used, which, according to the authors, was more suitable as catalyst support (EEG-Pt-eg, EEG-SnO_2@Pt) than other carbon materials since it has a small amount of oxygen-containing functional groups and defects on the surface. All presented methods of synthesis were complex, and the resulting materials were used as gas-sensitive materials in gas sensors or in DMFC.

In the present work, a cathode electrocatalyst for PEMFC was studied. RGO was used as a support to increase the electrical conductivity and ESA of the electrocatalyst. In this case, the durability and inhibition of the processes of corrosion for the support, as well as the dissolution and coarsening of Pt particles, were ensured by the formation of metal–metal oxide hetero-clusters of Pt-SnO_2. Both RGOs were preliminarily synthesized by thermal methods (t-RGO) and obtained by chemical reduction (c-RGO). The synthesis method saw a sequential reduction in component precursors to the final compound in a single content.

2. Results and Discussion

Figure 1 shows scanning electron microscopy (SEM) images (30 μm and 1 μm) of the studied electrocatalysts. On RGO samples obtained by thermal reduction (t-RGO), the layers of graphene sheets with a smooth, uniform surface were clearly pronounced. The

sample obtained by chemical reduction (c-RGO) is characterized more by the presence of RGO sheets (nanosized thickness) with agglomerates of amorphous carbon black. The sizes of amorphous carbon black agglomerates deposited on graphene-type structures were about 100–300 nm.

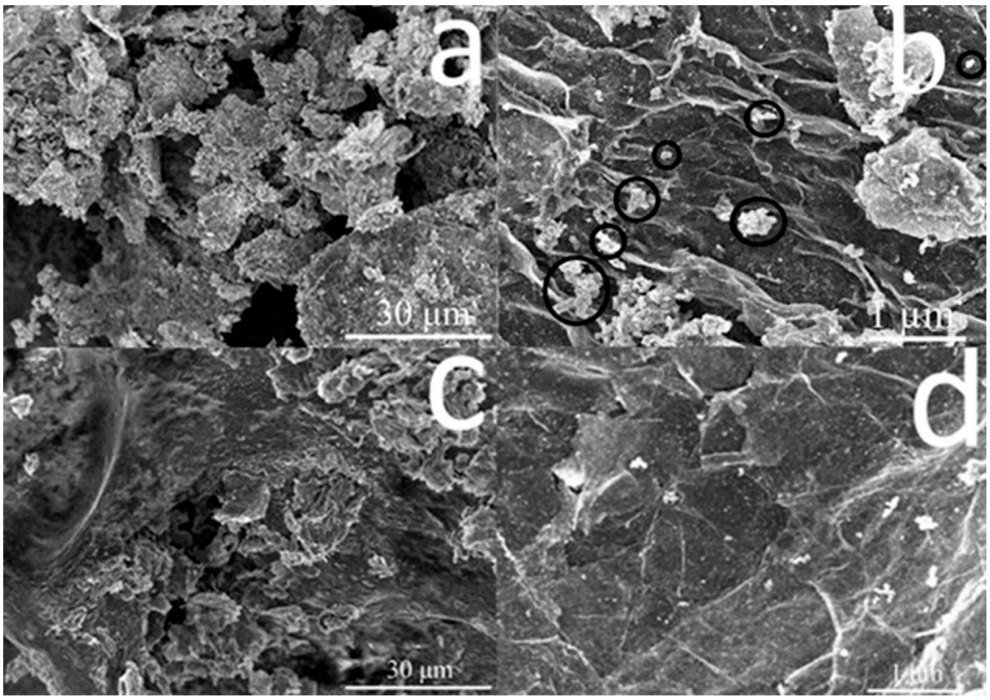

Figure 1. SEM images of electrocatalysts $Pt^{20}/SnO_2{}^{10}$/c-RGO (**a**,**b**), and $Pt^{20}/SnO_2{}^{10}$/t-RGO (**c**,**d**).

Figure 2 shows the transmission electron microscopy (TEM) images of $Pt^{20}/SnO_2{}^{10}$/c-RGO and $Pt^{20}/SnO_2{}^{10}$/t-RGO electrocatalysts, particle size distribution, and fast Fourier transform (FFT) images.

According to the results of previous studies [6], it was shown that it is the SnO_2 content of 10 wt.% that makes it possible to obtain a uniform distribution of particles without their significant agglomeration, which is also typical for samples based on RGO. Based on the analysis of the microphotograph (Figure 2), it was concluded that the particles were close to being spherical in shape and having a uniform distribution on the surface of the carbon support without large agglomerates. On high-resolution TEM images, a diffraction pattern can be distinguished in the form of parallel lines in image areas. Using FFT images, the interplanar spacing corresponding to Pt nanoparticles (0.22–0.23 nm) and SnO_2 particles (0.26–0.27 nm) was determined, which made it possible to compose the particle size distribution (Figure 2). The interplanar distance corresponding to the Pt-SnO_2 heterostructure (~0.2 nm) was also determined from the FFT image. The closeness of the lattice parameters did not allow us to isolate a specific interaction (Pt_3Sn and/or $Pt_{0.5}Sn_{0.5}$) but indicated the formation of heterostructures.

For the studied electrocatalysts, a close particle size distribution of Pt and SnO_2 was obtained. The average particle size of Pt was 2.1 nm ($Pt^{20}/SnO_2{}^{10}$/c-RGO) and 2.7 nm ($Pt^{20}/SnO_2{}^{10}$/t-RGO). For the electrocatalyst on c-RGO, a smaller size of platinum particles was observed, which could be associated with the synthesis of the electrocatalyst on reduced graphene oxide, as obtained by the chemical reduction method, and the presence of amorphous carbon black on the support surface. The average particle size of SnO_2 was 3.7 nm ($Pt^{20}/SnO_2{}^{10}$/c-RGO) and 3.3 nm ($Pt^{20}/SnO_2{}^{10}$/t-RGO).

The actual content of Pt and Sn in all catalysts was confirmed by energy-dispersive X-ray spectroscopy (EDX) measurements (Table 1, Figure 3). In the case of t-RGO, the distribution of SnO_2 was more scattered and could be associated with the composition of near-surface groups.

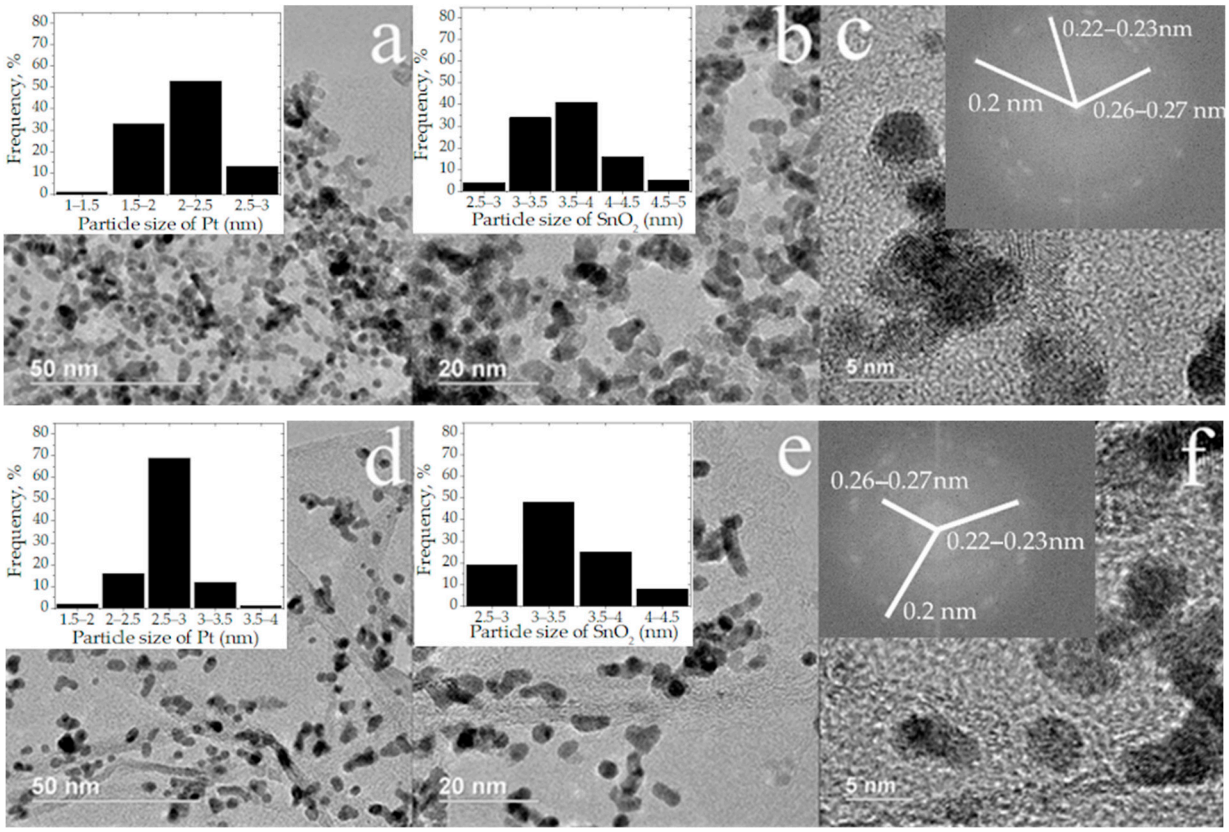

Figure 2. TEM images of $Pt^{20}/SnO_2{}^{10}$/c-RGO (**a**)—50 nm, (**b**)—20 nm, (**c**)—5 nm and $Pt^{20}/SnO_2{}^{10}$/t-RGO (**d**)—50 nm, (**e**)—20 nm, (**f**)—5 nm electrocatalysts and the particle size distribution of Pt and SnO_2. The insets show the corresponding Fourier-transformed diffraction patterns (**c**,**f**).

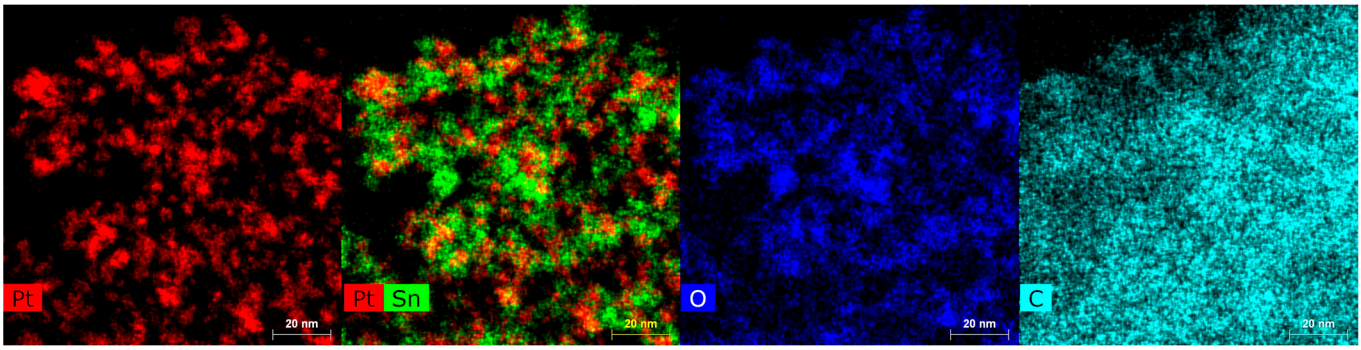

(**a**)

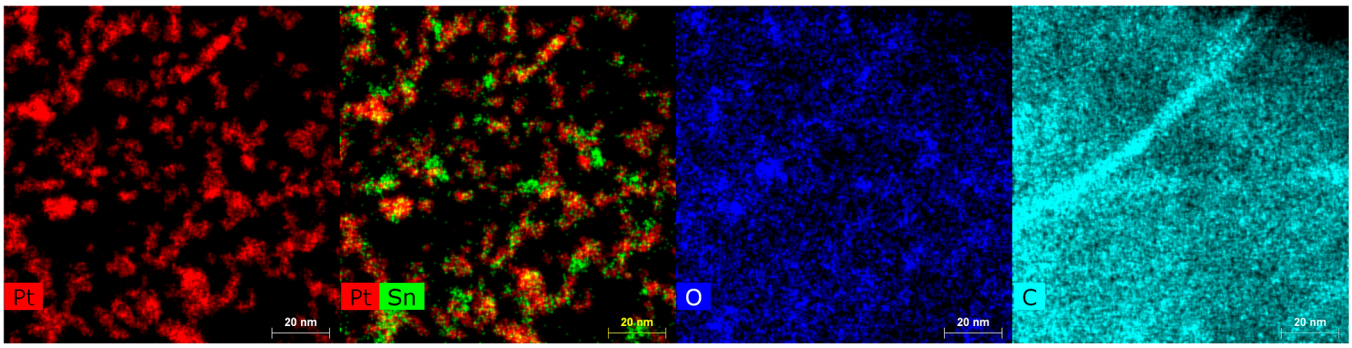

(**b**)

Figure 3. EDX map of $Pt^{20}/SnO_2{}^{10}$/c-RGO (**a**) and $Pt^{20}/SnO_2{}^{10}$/t-RGO (**b**) samples.

Table 1 presents the results of elemental analysis.

Table 1. Elemental analysis of samples.

Element	$Pt^{20}/SnO_2{}^{10}$/c-RGO	$Pt^{20}/SnO_2{}^{10}$/t-RGO	$Pt^{20}/SnO_2{}^{10}$/C [6]
C	64	67	67.5
Pt	17	17	20
Sn	9	8	8.5
O	10	9	4
SnO_2	11.5	9.8	10.7

The obtained values of the content of Pt and SnO_2 (the content of SnO_2 was calculated based on the assumption that 100% of tin was in the form of dioxide) were close for both samples and correlated with the objective of synthesizing electrocatalysts.

Figure 4 shows the diffraction patterns of the investigated electrocatalysts.

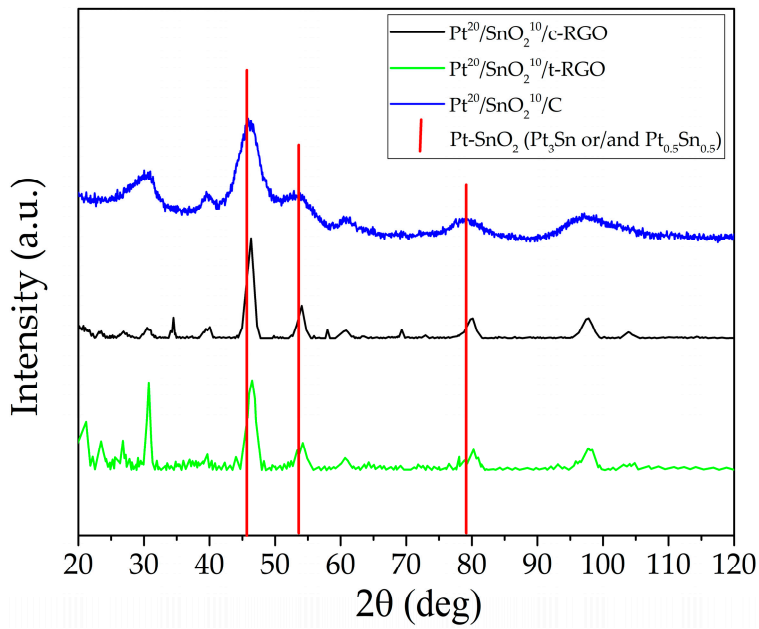

Figure 4. XRD pattern of $Pt^{20}/SnO_2{}^{10}$/c-RGO, $Pt^{20}/SnO_2{}^{10}$/t-RGO, and $Pt^{20}/SnO_2{}^{10}$/C [6] (the peaks of the lattice of Pt-SnO_2 heterostructures are marked with a red vertical line).

The diffraction peaks around 31°, 39°, and 61° refer to the SnO_2 planes. The diffraction peaks around 46°, 53°, 81°, and 96° are associated with the (111), (200), (220) and (331) Pt planes. The $Pt^{20}/SnO_2{}^{10}$/c-RGO and $Pt^{20}/SnO_2{}^{10}$/t-RGO samples were characterized by a peak at about 26°, which could be attributed to the RGO (002) graphite structure. The diffraction peak at 69.5° corresponds to the PtO phase and is present in all samples. PDF Cards are demonstrated in Figure S1.

According to the quantitative X-ray diffraction analysis for the $Pt^{20}/SnO_2{}^{10}$/c-RGO sample, the content of Pt_xSn_y phases was 10%, while in the $Pt^{20}/SnO_2{}^{10}$/t-RGO sample, it was only about 4%. The presence of Pt_xSn_y phases was indicated by the broadening of the peaks at about 46°, 53°, and 81°. The broadening of the peaks could also reflect an increase in the distance between platinum atoms in the lattice when the regularity of its structure was disturbed, including due to a surface interaction with heteroatoms. These effects were more pronounced for c-RGO.

XPS analysis was carried out in our previous work and was in good agreement with the literature data [6]. The SMSI effect in the prepared catalysts was induced by the formation of the Pt-SnO_2 clusters in which the electron donation from the oxide to Pt metal was observed. This enhanced electron density on the Pt metal, providing the higher activity and

stability of Pt nanoparticles. However, due to the low value of Pt $4f_{7/2}$, the binding energy shift was expected to be limited in its influence. Thus, the interaction between platinum and tin dioxide particles on the support surface was reflected by a low energy shift.

For samples of electrocatalysts, the curves of the Fourier transform modulus were obtained from the extended X-ray absorption fine structure (EXAFS) spectra (Figure 5), and the parameters of the atomic structure of Pt nanoparticles were estimated by fitting the model curve. Figure 5 shows the obtained experimental and model data.

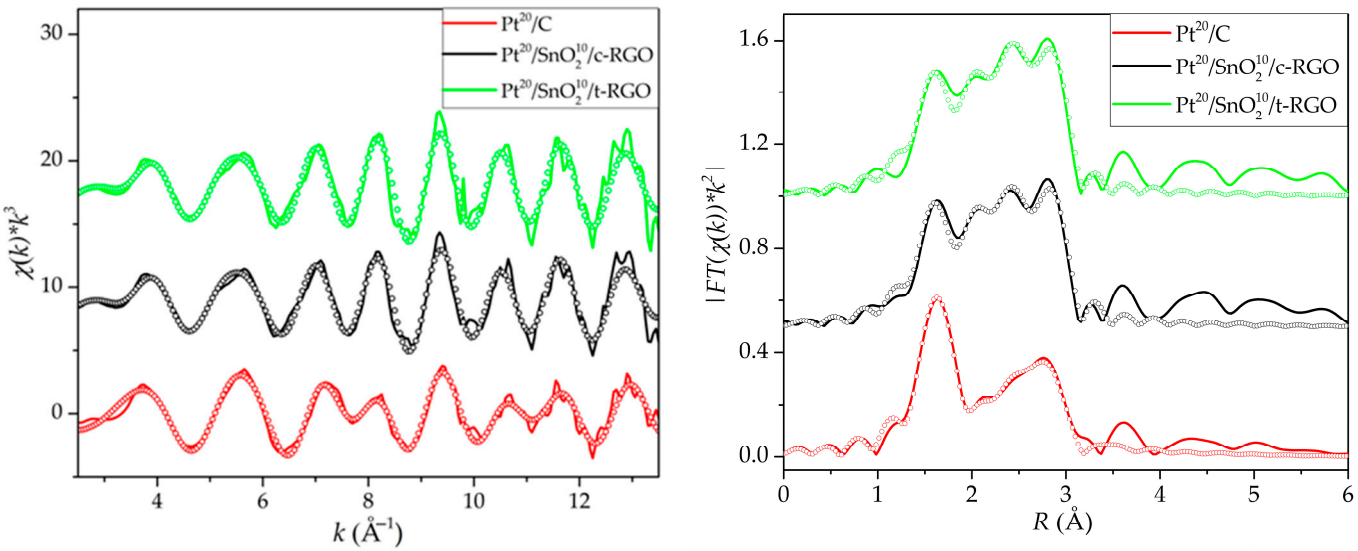

Figure 5. EXAFS at k and R space, respectively, for: Pt^{20}/C, $Pt^{20}/SnO_2{}^{10}$/c-RGO and $Pt^{20}/SnO_2{}^{10}$/t-RGO. Circles are theoretical data.

The parameters obtained during the fitting of the theoretical curve are shown in Table 2.

Table 2. Parameters of the theoretical curve. N is the coordination number; R is the distance from the central Pt atom to the neighboring atom.

	Pt^{20}/C		**$Pt^{20}/SnO_2{}^{10}$/c-RGO**		**$Pt^{20}/SnO_2{}^{10}$/t-RGO**	
Path	N	R, Å	N	R, Å	N	R, Å
$Pt\text{-}Pt_{(Pt\ foil)}$	4.1 ± 1.2	2.75	8.9 ± 1.6	2.75	9.0 ± 1.9	2.76
$Pt\text{-}O_{(PtO2)}$	2.6 ± 0.3	2.02	1.0 ± 0.3	2.00	1.2 ± 0.4	2.01
$Pt\text{-}Pt_{(PtO2)}$	2.6 ± 0.3	3.13	1.0 ± 0.3	3.07	1.2 ± 0.4	3.07

The large value of the $N_{Pt\text{-}O}$ number for the Pt^{20}/C sample indicated the inclusion of oxygen atoms in the structure of Pt nanoparticles. Samples with RGO showed a lower number of $N_{Pt\text{-}O}$, which indicated a better reduction in Pt in these samples. Samples with SnO_2 demonstrated a higher value of the coordination number of metallic Pt, which indicated a larger size of Pt nanoparticles due to agglomeration and competitive sorption with the modifier during synthesis. Wavelet transform of Pt L_3-edge EXAFS for Pt foil, PtO_2, Pt^{20}/C, $Pt^{20}/SnO_2{}^{10}$/c-RGO, and $Pt^{20}/SnO_2{}^{10}$/t-RGO are demonstrated on Figure S2. The analysis of EXAFS spectra using the Wavelet transform did not allow us to distinguish the explicit contribution of Pt-Sn, which probably indicated only the surface contact of particles in the composition of Pt-SnO_2 hetero-clusters.

To correlate these results, X-ray absorption near-edge structure (XANES) spectra were considered (Figure 6). As can be seen from the white line intensity, a larger amount of the oxide phase was present in the Pt^{20}/C sample.

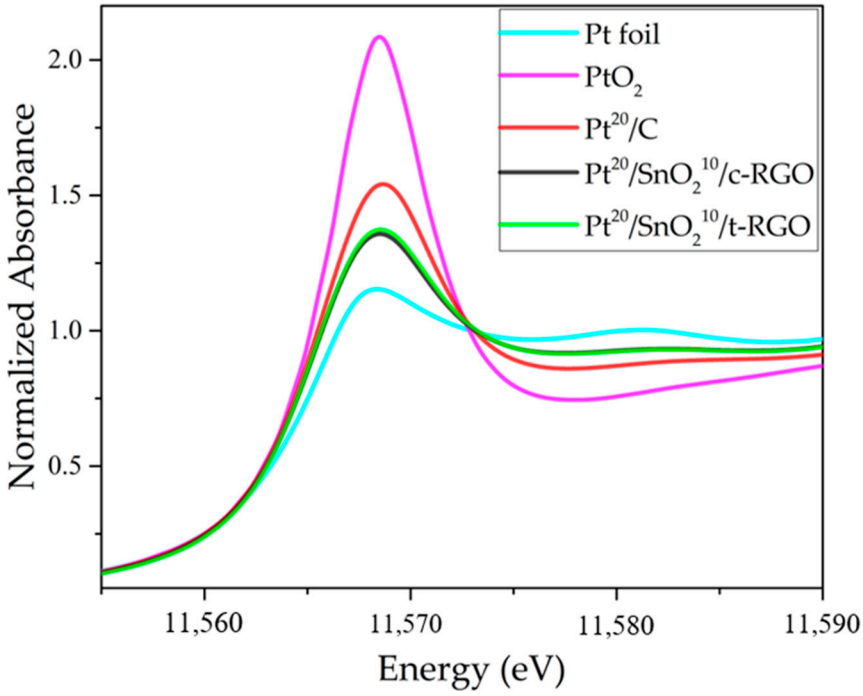

Figure 6. XANES spectra of the studied samples.

The white line peak of the XANES spectrum could also be represented as a linear combination of the Pt foil and PtO_2 spectra. Table 3 shows the percentage contributions of the spectra of the reference samples to the spectra of the studied samples. The larger linear contribution of Pt foil to the spectrum for RGO-based samples could also indicate electron donation from the oxide (SnO_2) to the Pt metal. This effect was reflected by Pt-catalysts based on the SnO_2-C supports [33]. In the case of Pt_3Sn/C electrocatalysts, an increase in the Pt 5d-orbital vacancy due to the redistribution of Pt 5d electrons to the low-energy 4d orbital of Sn could be observed [34].

Table 3. Contributions of Pt foil and PtO_2 to the white line intensity of the samples.

Catalysts	Pt Foil, %	PtO_2, %
Pt^{20}/C	52.5	47.5
$Pt^{20}/SnO_2{}^{10}$/c-RGO	74.5	25.5
$Pt^{20}/SnO_2{}^{10}$/t-RGO	72.5	27.5

The results of the performed analyses indicate the formation of Pt-SnO_2 hetero-clusters mainly for the $Pt^{20}/SnO_2{}^{10}$/c-RGO sample, and the interaction of particles had more surface in nature and was based on the inclusion of tin atoms in the surface structure of Pt particles with the formation of a distorted crystal lattice corresponding to broadening platinum peaks in the diffraction pattern. Broadening picks could be mistakenly associated with corresponding Pt_xSn_y phases (Pt_3Sn and/or $Pt_{0.5}Sn_{0.5}$).

Figure 7 shows the cyclic voltammograms (CVs) of the studied $Pt^{20}/SnO_2{}^{10}$/c-RGO, $Pt^{20}/SnO_2{}^{10}$/t-RGO, Pt^{20}/C, and $Pt^{20}/SnO_2{}^{10}$/C [6] samples.

The deposition density, as well as the conditions for the synthesis of Pt and SnO_2 particles, were identical for all samples; therefore, the difference between the current density of the double-layer region characterized diverse types of support. The larger current in the double-layer region reflected the high specific surface area of the RGO. As can be seen from the results of electrochemical studies, the use of RGO made it possible to significantly increase the ESA due to the larger specific surface area compared to a catalyst based on amorphous soot. The ESA of the $Pt^{20}/SnO_2{}^{10}$/c-RGO electrocatalyst was 1.5 times higher than that of the $Pt^{20}/SnO_2{}^{10}$/C [6] electrocatalyst (Table 4).

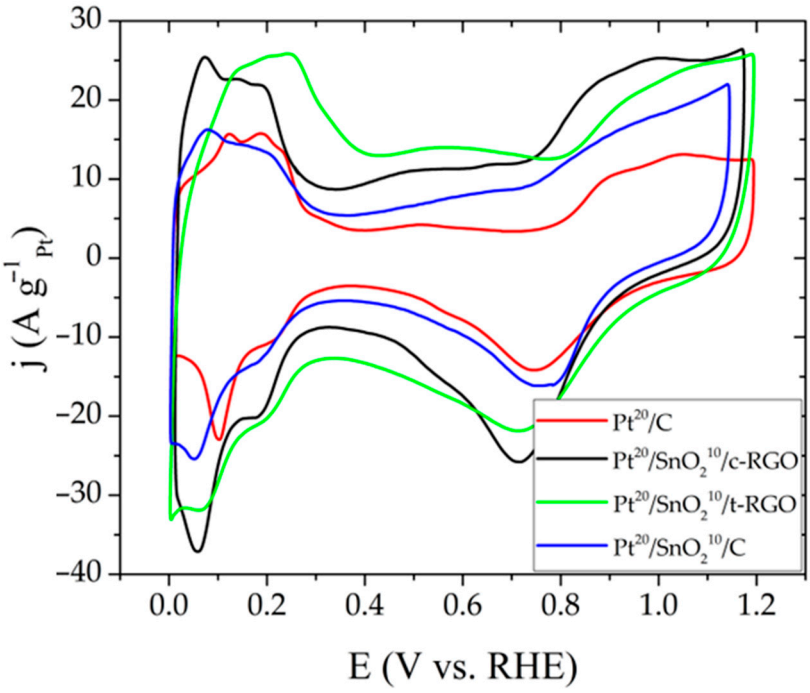

Figure 7. CVs of Pt^{20}/C, $Pt^{20}/SnO_2{}^{10}$/c-RGO, $Pt^{20}/SnO_2{}^{10}$/t-RGO and $Pt^{20}/SnO_2{}^{10}/C$ [6] recorded in N_2-saturateted 0.5 M H_2SO_4 solution at a potential sweep rate of 20 mV/s.

Table 4. ESA values before and after AST.

Catalysts	ESA, $m^2\ g^{-1}$	ESA after AST, $m^2\ g^{-1}$
Pt^{20}/C	62	25
$Pt^{20}/SnO_2{}^{10}$/c-RGO	85	52
$Pt^{20}/SnO_2{}^{10}$/t-RGO	72	5
$Pt^{20}/SnO_2{}^{10}/C$ [6]	57	35

Figure 8 presents the results of the AST. For all catalysts, there was a gradual decrease in the ESA values associated with the agglomeration and separation of Pt particles, as well as the degradation of the carbon support. For the sample on t-RGO, the ESA loss was 92–94%. A sharp drop in ESA for t-RGO was associated with the destruction of the electrocatalyst due to the oxidation and corrosion of the support due to the presence of oxygen groups on the surface of the carbon structure. In turn, the precipitated SnO_2 particles for t-RGO catalyzed the oxidation processes and accelerated the destruction in graphene under the action of high potentials, even when compared with Pt/RGO catalysts [35]. At the same time, the protective effect of applying SnO_2 was not pronounced due to the absence of particle interactions.

The $Pt^{20}/SnO_2{}^{10}$/c-RGO and $Pt^{20}/SnO_2{}^{10}/C$ [6] samples showed the highest stability in AST cycles. The loss was no more than 40%. Thus, the chemical composition of the surface of c-RGO obtained by chemical reduction made it possible to achieve the formation of stable heterostructures, which significantly increased the lifetime of the catalyst, as in the case of using amorphous carbon black, while the ESA was 1.5 times higher. Figure S3 shows the change in CVs during the AST process.

Polarization curves of the $Pt^{20}/SnO_2{}^{10}$/c-RGO were recorded in an O_2-saturated 0.1 M $HClO_4$ solution on the glassy carbon electrode with an area of 0.102 cm^2 at rotating rates ranging from 500 to 1200 rpm and a scan rate of 10 mV s^{-1} (Figure 9). The mass (M_a) and specific (S_a) activities of the $Pt^{20}/SnO_2{}^{10}$/c-RGO in the oxygen reduction reaction were 0.23 mA cm^{-2} and 192 mA mg^{-1}, respectively. Compared with Pt^{20}/C (S_a = 0.25 mA cm^{-2}, M_a = 207 mA mg^{-1} [7]), $Pt^{20}/SnO_2{}^{10}$/c-RGO showed slightly lower activities due to the close packing of RGO sheets, making it difficult for oxygen to diffuse into the active

sites [36]. The catalysts modified with tin dioxide demonstrated high activity despite the partial blockage of Pt active sites by SnO_2 nanoparticles. The relatively high activity of the composite catalyst was explained by the participation of tin dioxide in the ORR as a co-catalyst. Thus, both platinum and tin dioxide particles are emphasized as active sites [7].

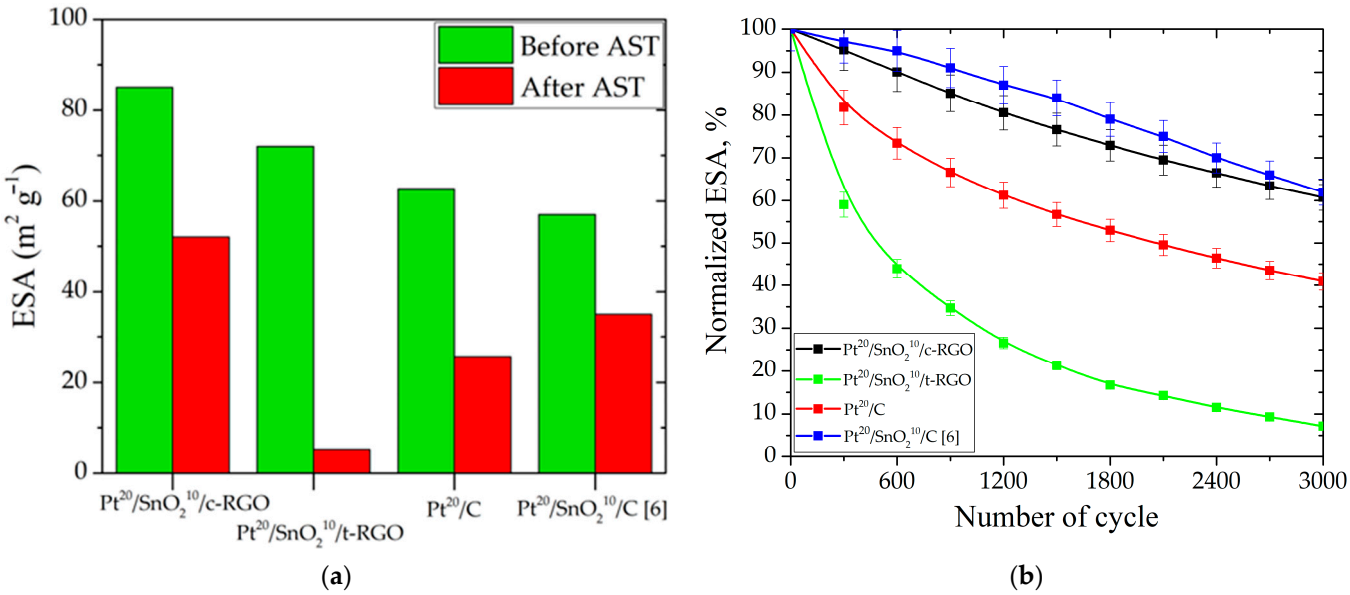

Figure 8. ESA values before and after AST (**a**) and loss of normalized ESA during AST (**b**).

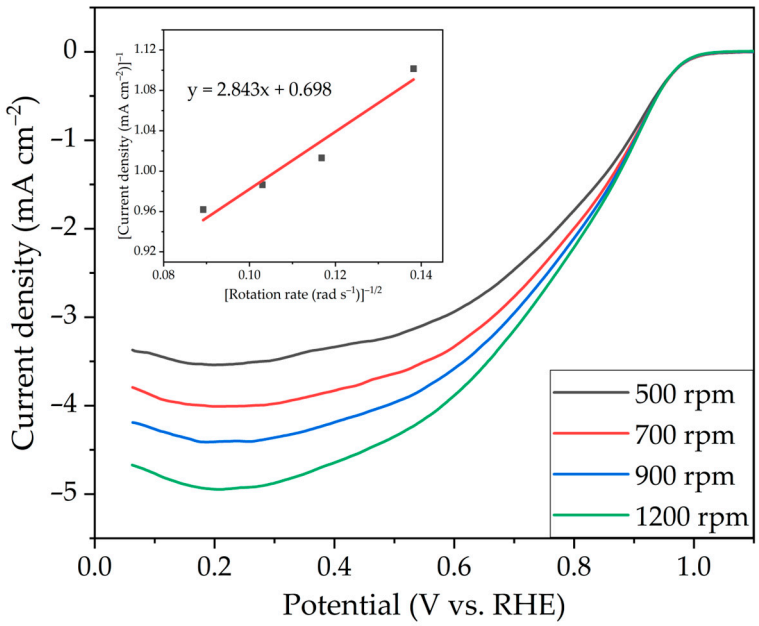

Figure 9. Polarization curves of $Pt^{20}/SnO_2{}^{10}$/c-RGO with different RDE rotation rates in O_2-saturated 0.1 M $HClO_4$ solution. The inset shows the corresponding Koutecky–Levich plot at 0.9 V.

3. Materials and Methods

3.1. Preparation of Pt/SnO₂(Sn)/GRO Catalysts

The first step in the synthesis of a multicomponent catalyst is the preparation of a sol of Sn/SnO_2 nanoparticles according to the procedure described in detail in [6]. Reduced graphene oxide was used as a carbon support for the synthesis. Graphite oxide and thermally reduced graphene oxide (t-RGO) are provided by the Semenov Institute of Chemical Physics of Russian Academy of Sciences, Russia. The synthesis of graphite

oxide was carried out according to the modified Hummers method. t-RGO was obtained according to the procedure presented in [37].

The chemical reduction in graphite oxide to c-RGO was carried out in a volume of ethylene glycol at a temperature of 180 °C; for 2 h in an argon atmosphere with the constant stirring of the solution. The finished media was washed and dried in a vacuum oven at 70 °C for 2 h.

Then, Sn/SnO_2 particles were absorbed into the preliminarily synthesized support as described in [6]. The sorption of the H_2PtCl_6 precursor of Pt particles and then the chemical reduction of Pt in metal particles was carried out by the polyol method in the volume of ethylene glycol [6]. The finished catalyst was washed and dried in a vacuum oven at 70 °C for 2 h.

3.2. Structural and Morphological Studies

The study of the phase composition of the samples was carried out at the Belok/XSA beamline of the specialized source of synchrotron radiation "KISI-Kurchatov" [38] and was equipped with a Rayonix SX165 two-dimensional CCD detector.

The measurements were carried out at room temperature. The survey was carried out in transmission geometry. The distance between the sample and the detector was 150 mm, and the tilt angle was 29.5° from the direct beam axis to maximize the angular scale. The size of the photon beam was 400 × 400 μm^2. The shooting time for one sample was 5 min. The spectra were recalculated considering the wavelength WL = 1.7889.

The samples were examined by SEM using a Versa 3D DualBeam instrument (FEI, Hillsboro, OR, USA). Additionally, an FEI Osiris transmission electron microscope (equipment of the Center of Collective Use of the Federal Scientific Research Centre «Crystallography and Photonics» of the Russian Academy of Sciences, Moscow, Russia) was used.

The particle size distribution data and FFT image were obtained through the processing of the TEM images with ImageJ software, considering more than 1000 particles.

The Extended X-ray Absorption Fine Structure and X-ray Absorption Near Edge Structure (EXAFS and Pt L3 XANES) measurements of electrocatalysts were performed at the Structural Materials Science beamline of the National Research Center "Kurchatov Institute" (Moscow) in the transmission mode. The EXAFS structural analysis was performed using theoretical phases and amplitudes, as calculated by the FEFF-9 package [39], which fit the experimental data and were carried out in R-space with the IFFEFIT package [40].

3.3. Electrochemical Studies

Catalytic inks were prepared by mixing 10 mg of electrocatalyst with 1 mL of a 1:1 isopropanol/water solution, followed by ultrasonication for half an hour at room temperature. Then, the resulting catalytic ink aliquot with a volume of 25 µL was pipetted onto a polished and cleaned titanium foil electrode with a geometric area of 0.5 cm^2, forming a thin catalyst layer. After that, the titanium electrode was dried until the solvent was completely removed. The final catalyst loading was about 0.5 mg cm^{-2}.

The CVs were measured in N_2-saturated 0.5 M H_2SO_4 at 25 °C using a conventional three-electrode glass cell, an RHE reference electrode, and a Pt wire counter electrode. The measurements were performed using a CorrTest CS350 electrochemical workstation (CorrTest Instruments Corp., Ltd., Wuhan, China). Before CV registration, the electrode was activated at a potential range of 0.05 to 1.20 V vs. RHE and was maintained at the 50 mV/s potential sweep rate for about 30 cycles until a stable CV was obtained. The CVs of all samples were recorded at the same sweep rate of 20 mV/s in the same potential range and were then normalized according to the total mass of Pt in the catalyst layer.

Electrocatalysts were subjected to an AST [41,42] by cycling potential in the range of 0.8–1.4 V vs. the RHE electrode with a sweep rate of 100 mV/s for 3000 cycles. A working 0.5 M H_2SO_4 solution was pre-saturated with oxygen before AST cycles. CVs were measured initially and every 300 cycles. Before the CVs measurement, the working

solution was saturated with N_2. The degree of degradation of the catalyst was estimated from the change in the ESA, which was calculated from the CVs.

Activity in the oxygen reduction reaction (ORR) was determined by rotating disk electrode methods in 0.1 M $HClO_4$. The technique for studying the activity of electrocatalysts in the ORR is described in detail in [7].

4. Conclusions

Various structural studies were carried out to determine the nature of the interaction between Pt and SnO_2 particles on the RGO-support surface. Combining the results of the XRD method and EXAFS method, no formation of Pt_3Sn or $Pt_{0.5}Sn_{0.5}$ phases in the composition of the electrocatalyst was observed since there was a surface interaction of the crystal lattices of platinum and tin oxide particles due to their proximity contact on the RGO-surface and the formation of Pt-SnO_2 hetero-clusters which mostly reflected the $Pt^{20}/SnO_2{}^{10}$/c-RGO electrocatalyst. This achieved high dispersity during the formation of platinum particles without a significant agglomeration (average size about 2.1 nm) and obtained high ESA values of 85 m^2g^{-1}. The TEM images show a uniform distribution over the surface of both Pt and SnO_2 particles.

Electrochemical studies have shown the advantages of using chemically reduced RGO as a carrier for Pt-SnO_2 hetero-clusters compared to thermal reduced RGO and amorphous carbon black.

The near-surface incorporation of SnO_2 particles into the crystal lattice of Pt particles protected electrocatalysts from degradation during the accelerate stress test. The drop in ESA for the $Pt^{20}/SnO_2{}^{10}$/c-RGO sample was only 40%. The decrease in ESA for electrocatalysts based on t-RGO was about 95% and could be associated with the destruction of the electrocatalyst due to the oxidation and corrosion of the support due to the presence of oxygen groups on the surface of the carbon structure.

The $Pt^{20}/SnO_2{}^{10}$/c-RGO electrocatalyst had the highest ESA, high stability, and similar activity in ORR compared to Pt^{20}/C and could be proposed as an efficient cathode catalyst for PEMFC.

Supplementary Materials: The following supporting information can be downloaded at: https://www.mdpi.com/article/10.3390/inorganics11080325/s1, Figure S1: XRD pattern of $Pt^{20}/SnO_2{}^{10}$/c-RGO and PDF card ($Pt_{0.5}Sn_{0.5}$, Pt_3Sn, SnO_2); Figure S2: Wavelet transform of Pt L_3-edge EXAFS for Pt foil, PtO_2, Pt^{20}/C, $Pt^{20}/SnO_2{}^{10}$/c-RGO and $Pt^{20}/SnO_2{}^{10}$/t-RGO; Figure S3: Changing CVs during AST samples Pt^{20}/C (a), $Pt^{20}/SnO_2{}^{10}$/t-RGO (b) and $Pt^{20}/SnO_2{}^{10}$/c-RGO (c).

Author Contributions: Conceptualization, N.A.I., R.M.M., D.D.S. and V.N.F.; methodology, R.M.M., E.V.K., D.D.S., M.V.S., A.A.Z., E.S.K. and A.L.T.; software, R.M.M. and D.D.S.; validation, N.A.I. and V.N.F.; investigation, D.D.S., R.M.M., N.A.I. and M.V.S.; resources, V.N.F.; writing—original draft preparation, D.D.S., R.M.M. and N.A.I.; writing—review and editing, D.D.S., R.M.M. and N.A.I.; visualization, D.D.S., N.A.I. and R.M.M.; supervision, N.A.I. and V.N.F.; project administration, V.N.F. and N.A.I.; funding acquisition, V.N.F. All authors have read and agreed to the published version of the manuscript.

Funding: The work was carried out at the National Research Center "Kurchatov Institute" in the framework of execution of Order No. 89 dated 20 January 2023, item 3p.2.5. "Development of new electrocatalytic materials with improved properties for PEM electrochemical devices".

Data Availability Statement: The data presented in this study are available on request from the corresponding author.

Conflicts of Interest: The authors declare no conflict of interest.

References

1. Liu, J.; Takeshi, D.; Sasaki, K.; Lyth, S.M. Defective Graphene Foam: A Platinum Catalyst Support for PEMFCs. *J. Electrochem. Soc.* **2014**, *161*, F838. [CrossRef]
2. Yin, M.; Xu, J.; Li, Q.; Jensen, J.O.; Huang, Y.; Cleemann, L.N.; Bjerrum, N.J.; Xing, W. Highly Active and Stable Pt Electrocatalysts Promoted by Antimony-Doped SnO_2 Supports for Oxygen Reduction Reactions. *Appl. Catal. B Environ.* **2014**, *144*, 112–120. [CrossRef]
3. Ignaszak, A.; Teo, C.; Ye, S.; Gyenge, E. Pt-SnO_2-Pd/C Electrocatalyst with Enhanced Activity and Durability for the Oxygen Reduction Reaction at Low Pt Loading: The Effect of Carbon Support Type and Activation. *J. Phys. Chem. C* **2010**, *114*, 16488–16504. [CrossRef]
4. Xu, J.; Aili, D.; Li, Q.; Pan, C.; Christensen, E.; Jensen, J.O.; Zhang, W.; Liu, G.; Wang, X.; Bjerrum, N.J. Antimony Doped Tin Oxide Modified Carbon Nanotubes as Catalyst Supports for Methanol Oxidation and Oxygen Reduction Reactions. *J. Mater. Chem. A* **2013**, *1*, 9737–9745. [CrossRef]
5. Nakazato, Y.; Kawachino, D.; Noda, Z.; Matsuda, J.; Lyth, S.M.; Hayashi, A.; Sasaki, K. PEFC Electrocatalysts Supported on Nb-SnO_2 for MEAs with High Activity and Durability: Part I. Application of Different Carbon Fillers. *J. Electrochem. Soc.* **2018**, *165*, F1154. [CrossRef]
6. Spasov, D.D.; Ivanova, N.A.; Pushkarev, A.S.; Pushkareva, I.V.; Presnyakova, N.N.; Chumakov, R.G.; Presnyakov, M.Y.; Grigoriev, S.A.; Fateev, V.N. On the Influence of Composition and Structure of Carbon-Supported Pt-SnO_2 Hetero-Clusters onto Their Electrocatalytic Activity and Durability in PEMFC. *Catalysts* **2019**, *9*, 803. [CrossRef]
7. Mensharapov, R.M.; Ivanova, N.A.; Spasov, D.D.; Kukueva, E.V.; Zasypkina, A.A.; Seregina, E.A.; Grigoriev, S.A.; Fateev, V.N. Carbon-Supported Pt-SnO_2 Catalysts for Oxygen Reduction Reaction over a Wide Temperature Range: Rotating Disk Electrode Study. *Catalysts* **2021**, *11*, 1469. [CrossRef]
8. Trogadas, P.; Fuller, T.F.; Strasser, P. Carbon as Catalyst and Support for Electrochemical Energy Conversion. *Carbon* **2014**, *75*, 5–42. [CrossRef]
9. Hummers, W.S., Jr.; Offeman, R.E. Preparation of Graphitic Oxide. *J. Am. Chem. Soc.* **1958**, *80*, 1339. [CrossRef]
10. Marcano, D.C.; Kosynkin, D.V.; Berlin, J.M.; Sinitskii, A.; Sun, Z.; Slesarev, A.; Alemany, L.B.; Lu, W.; Tour, J.M. Improved Synthesis of Graphene Oxide. *ACS Nano* **2010**, *4*, 4806–4814. [CrossRef] [PubMed]
11. Choi, W.; Lahiri, I.; Seelaboyina, R.; Kang, Y.S. Synthesis of Graphene and Its Applications: A Review. *Crit. Rev. Solid State Mater. Sci.* **2010**, *35*, 52–71. [CrossRef]
12. Chae, S.J.; Güneş, F.; Kim, K.K.; Kim, E.S.; Han, G.H.; Kim, S.M.; Shin, H.-J.; Yoon, S.-M.; Choi, J.-Y.; Park, M.H. Synthesis of Large-Area Graphene Layers on Poly-Nickel Substrate by Chemical Vapor Deposition: Wrinkle Formation. *Adv. Mater.* **2009**, *21*, 2328–2333. [CrossRef]
13. Chua, C.K.; Pumera, M. Chemical Reduction of Graphene Oxide: A Synthetic Chemistry Viewpoint. *Chem. Soc. Rev.* **2014**, *43*, 291–312. [CrossRef] [PubMed]
14. De Silva, K.K.H.; Huang, H.-H.; Joshi, R.; Yoshimura, M. Restoration of the Graphitic Structure by Defect Repair during the Thermal Reduction of Graphene Oxide. *Carbon* **2020**, *166*, 74–90. [CrossRef]
15. El-Hallag, I.S.; El-Nahass, M.N.; Youssry, S.M.; Kumar, R.; Abdel-Galeil, M.M.; Matsuda, A. Facile In-Situ Simultaneous Electrochemical Reduction and Deposition of Reduced Graphene Oxide Embedded Palladium Nanoparticles as High Performance Electrode Materials for Supercapacitor with Excellent Rate Capability. *Electrochim. Acta* **2019**, *314*, 124–134. [CrossRef]
16. Xie, X.; Zhou, Y.; Huang, K. Advances in Microwave-Assisted Production of Reduced Graphene Oxide. *Front. Chem.* **2019**, *7*, 355. [CrossRef]
17. Meng, H.-B.; Zhang, X.-F.; Pu, Y.-L.; Chen, X.-L.; Feng, J.-J.; Han, D.-M.; Wang, A.-J. One-Pot Solvothermal Synthesis of Reduced Graphene Oxide-Supported Uniform PtCo Nanocrystals for Efficient and Robust Electrocatalysis. *J. Colloid Interface Sci.* **2019**, *543*, 17–24. [CrossRef]
18. Joshi, D.J.; Koduru, J.R.; Malek, N.I.; Hussain, C.M.; Kailasa, S.K. Surface Modifications and Analytical Applications of Graphene Oxide: A Review. *TrAC Trends Anal. Chem.* **2021**, *144*, 116448. [CrossRef]
19. Wang, Y.; Wang, D.; Li, Y. A Fundamental Comprehension and Recent Progress in Advanced Pt-Based ORR Nanocatalysts. *SmartMat* **2021**, *2*, 56–75. [CrossRef]
20. Seselj, N.; Engelbrekt, C.; Zhang, J. Graphene-Supported Platinum Catalysts for Fuel Cells. *Sci. Bull.* **2015**, *60*, 864–876. [CrossRef]
21. Yadav, R.; Subhash, A.; Chemmenchery, N.; Kandasubramanian, B. Graphene and Graphene Oxide for Fuel Cell Technology. *Ind. Eng. Chem. Res.* **2018**, *57*, 9333–9350. [CrossRef]
22. Marinoiu, A.; Carcadea, E.; Sacca, A.; Carbone, A.; Sisu, C.; Dogaru, A.; Raceanu, M.; Varlam, M. One-Step Synthesis of Graphene Supported Platinum Nanoparticles as Electrocatalyst for PEM Fuel Cells. *Int. J. Hydrogen Energy* **2021**, *46*, 12242–12253. [CrossRef]
23. Navazani, S.; Shokuhfar, A.; Hassanisadi, M.; Di Carlo, A.; Nia, N.Y.; Agresti, A. A PdPt Decorated SnO_2-RGO Nanohybrid for High-Performance Resistive Sensing of Methane. *J. Taiwan Inst. Chem. Eng.* **2019**, *95*, 438–451. [CrossRef]
24. Kim, J.-H.; Zheng, Y.; Mirzaei, A.; Kim, H.W.; Kim, S.S. Synthesis and Selective Sensing Properties of RGO/Metal-Coloaded SnO_2 Nanofibers. *J. Electron. Mater.* **2017**, *46*, 3531–3541. [CrossRef]
25. Bhangare, B.; Sinju, K.R.; Ramgir, N.S.; Gosavi, S.; Debnath, A.K. Noble Metal Sensitized SnO_2/RGO Nanohybrids as Chemiresistive E-Nose for H2, H2S and NO_2 Detection. *Mater. Sci. Semicond. Process.* **2022**, *147*, 106706. [CrossRef]

26. Peng, R.; Chen, J.; Nie, X.; Li, D.; Si, P.; Feng, J.; Zhang, L.; Ci, L. Reduced Graphene Oxide Decorated Pt Activated SnO_2 Nanoparticles for Enhancing Methanol Sensing Performance. *J. Alloys Compd.* **2018**, *762*, 8–15. [CrossRef]
27. Wu, S.; Liu, J.; Ye, Y.; Tian, Z.; Zhu, X.; Liang, C. Oxygen Defects Induce Strongly Coupled Pt/Metal Oxides/RGO Nanocomposites for Methanol Oxidation Reaction. *ACS Appl. Energy Mater.* **2019**, *2*, 5577–5583. [CrossRef]
28. Aryafar, A.; Ekrami-Kakhki, M.-S.; Naeimi, A. Enhanced Electrocatalytic Activity of Pt-SnO_2 Nanoparticles Supported on Natural Bentonite-Functionalized Reduced Graphene Oxide-Extracted Chitosan from Shrimp Wastes for Methanol Electro-Oxidation. *Sci. Rep.* **2023**, *13*, 3597. [CrossRef]
29. Xu, P.; Zhao, S.; Wang, T.; Ji, W.; Chen, Z.; Au, C.-T. A Pt/SnO 2/RGO Interface More Capable of Converting Ethanol to CO_2 in Ethanol Electro-Oxidation: A Detailed Experimental/DFT Study. *J. Mater. Chem. A* **2022**, *10*, 10150–10161. [CrossRef]
30. Wu, S.; Liu, J.; Liang, D.; Sun, H.; Ye, Y.; Tian, Z.; Liang, C. Photo-Excited in Situ Loading of Pt Clusters onto RGO Immobilized SnO_2 with Excellent Catalytic Performance toward Methanol Oxidation. *Nano Energy* **2016**, *26*, 699–707. [CrossRef]
31. Wang, H.; Zhang, K.; Qiu, J.; Wu, J.; Shao, J.; Deng, Y.; Wu, Y.; Yan, L. Photoassisted Reduction Synthesis of Pt@ SnO_2/Graphene Catalysts with Excellent Activities toward Methanol Oxidation. *Energy Fuels* **2021**, *35*, 12516–12526. [CrossRef]
32. Yuan, X.; Yue, W.-B.; Zhang, J. Electrochemically exfoliated graphene as high-performance catalyst support to promote electrocatalytic oxidation of methanol on Pt catalysts. *J. Cent. South Univ.* **2020**, *27*, 2515–2529. [CrossRef]
33. Hussain, S.; Kongi, N.; Erikson, H.; Rähn, M.; Merisalu, M.; Matisen, L.; Paiste, P.; Aruväli, J.; Sammelselg, V.; Estudillo-Wong, L.A. Platinum Nanoparticles Photo-Deposited on SnO_2-C Composites: An Active and Durable Electrocatalyst for the Oxygen Reduction Reaction. *Electrochim. Acta* **2019**, *316*, 162–172. [CrossRef]
34. Su, B.-J.; Wang, K.-W.; Tseng, C.-J.; Pao, C.-W.; Chen, J.-L.; Lu, K.-T.; Chen, J.-M. High Durability of Pt3Sn/Graphene Electrocatalysts toward the Oxygen Reduction Reaction Studied with in Situ QEXAFS. *ACS Appl. Mater. Interfaces* **2020**, *12*, 24710–24716. [CrossRef]
35. Pushkareva, I.V.; Pushkarev, A.S.; Kalinichenko, V.N.; Chumakov, R.G.; Soloviev, M.A.; Liang, Y.; Millet, P.; Grigoriev, S.A. Reduced Graphene Oxide-Supported Pt-Based Catalysts for PEM Fuel Cells with Enhanced Activity and Stability. *Catalysts* **2021**, *11*, 256. [CrossRef]
36. Li, Y.; Li, Y.; Zhu, E.; McLouth, T.; Chiu, C.-Y.; Huang, X.; Huang, Y. Stabilization of High-Performance Oxygen Reduction Reaction Pt Electrocatalyst Supported on Reduced Graphene Oxide/Carbon Black Composite. *J. Am. Chem. Soc.* **2012**, *134*, 12326–12329. [CrossRef]
37. Grigoriev, S.A.; Fateev, V.N.; Pushkarev, A.S.; Pushkareva, I.V.; Ivanova, N.A.; Kalinichenko, V.N.; Yu, P.; Resnyakov, M.; Wei, X. Reduced Graphene Oxide and Its Modifications as Catalyst Supports and Catalyst Layer Modifiers for PEMFC. *Materials* **2018**, *11*, 1405. [CrossRef]
38. Svetogorov, R.; Dorovatovskii, P.V.; Lazarenko, V.A. Belok/XSA Diffraction Beamline for Studying Crystalline Samples at Kurchatov Synchrotron Radiation Source. *Cryst. Res. Technol.* **2020**, *55*, 1900184. [CrossRef]
39. Rehr, J.J.; Kas, J.J.; Vila, F.D.; Prange, M.P.; Jorissen, K. Parameter-free calculations of X-ray spectra with FEFF9. *Phys. Chem. Chem. Phys.* **2010**, *12*, 5503. [CrossRef]
40. Newville, M. IFEFFIT: Interactive XAFS analysis and FEFF fitting. *J. Synchrotron Radiat.* **2001**, *8*, 322–324. [CrossRef]
41. Mensharapov, R.M.; Spasov, D.D.; Ivanova, N.A.; Zasypkina, A.A.; Smirnov, S.A.; Grigoriev, S.A. Screening of Carbon-Supported Platinum Electrocatalysts Using Frumkin Adsorption Isotherms. *Inorganics* **2023**, *11*, 103. [CrossRef]
42. Ivanova, N.A.; Spasov, D.D.; Zasypkina, A.A.; Alekseeva, O.K.; Kukueva, E.V.; Vorobyeva, E.A.; Kudinova, E.S.; Chumakov, R.G.; Millet, P.; Grigoriev, S.A. Comparison of the Performance and Durability of PEM Fuel Cells with Different Pt-Activated Microporous Layers. *Int. J. Hydrogen Energy* **2021**, *46*, 18093–18106. [CrossRef]